Infrared Backscattering From the Atmosphere: Some Observations

By Madison J. Post

While studying the possibility of measuring vertical wind profiles from space using an infrared lidar (the WINDSAT[1] concept), NOAA became interested in the infrared backscattering properties of the atmosphere and their variability in time, altitude, and geographic location.

A three-year observation program in Boulder, Colo., using NOAA's trailer-mounted coherent Doppler lidar[2] at 10.6 μm wavelength has borne unexpected fruits. Besides quantifying seasonal means and variabilities for this continental environment, we have observed possible long-range transport of Gobi dust, determined backscatter to extinction ratios of cirrus clouds, and measured the appearance of the El Chichón stratospheric cloud and its dissipation into the troposphere.

We take data by pointing the lidar beam vertically and transmitting a 2 μsec-long pulse of coherent energy. The energy backscattered to the lidar is coherently detected on a HgCdTe chip illuminated by a frequency-offset local oscillator. The detector output is digitized at a rate of 10 MHz for 200 μs, letting us record the backscatter signal to altitudes of 30 km above the lidar.

However, such coherent signals are extremely noisy because of speckle, and standard deviations are equal to the mean even for high signal-to-noise ratios. To reduce the speckle noise and to suppress shot noise fluctuations induced by the local oscillator, we typically average 1000 pulses. Since the laser pulse repetition frequency is 10 Hz, this represents a 100-second temporal

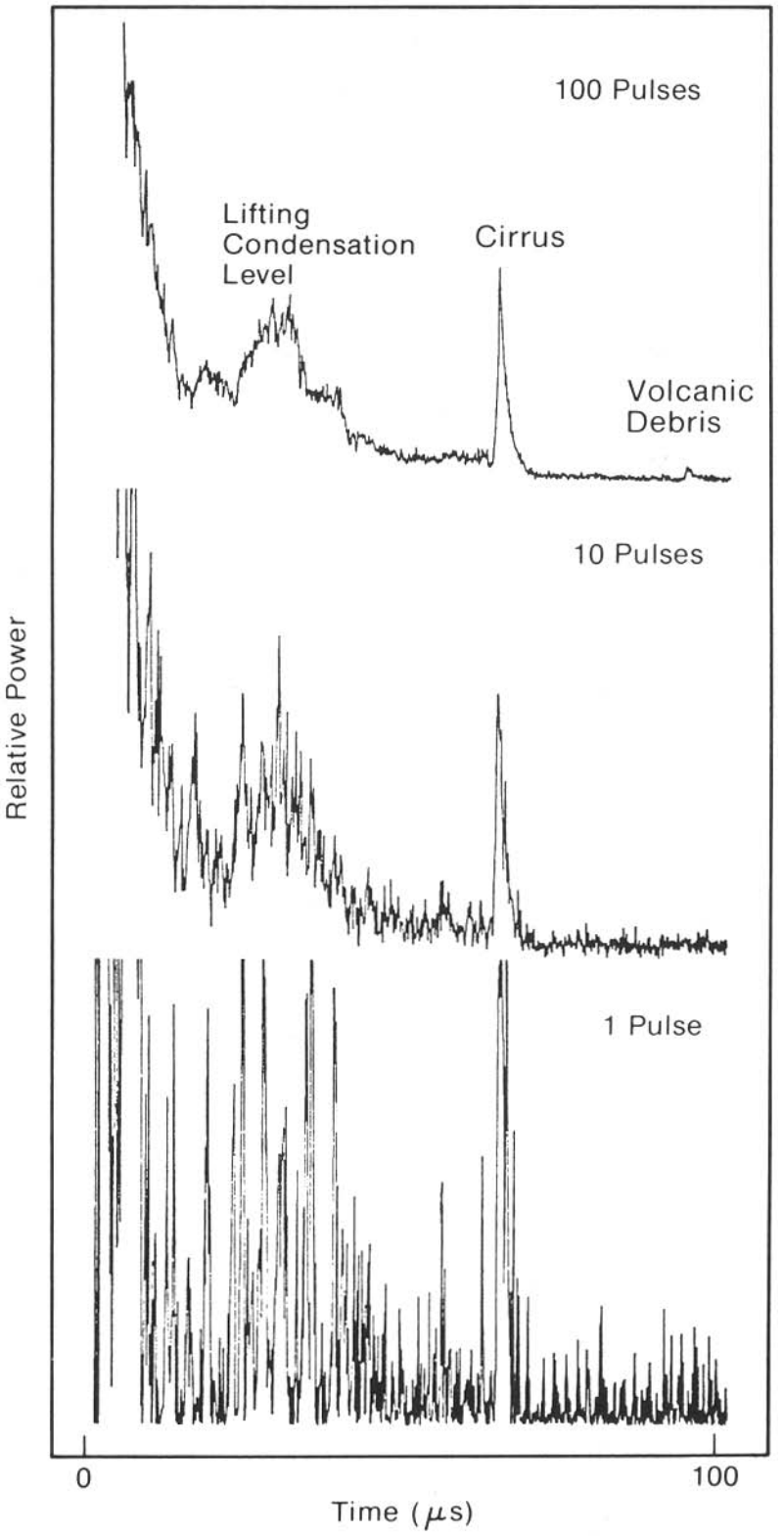

Fig. 1. Reduction of speckle noise by averaging multiple pulses. Recorded signal level (arbitrary units) is vertical, time (in microseconds) or range (150 m μs^{-1}) is horizontal.

Madison J. Post is with the Atmospheric Lidar Program at the Wave Propagation Laboratory—part of the Environmental Research Laboratories, National Oceanic and Atmospheric Administration, Boulder, Colo. This paper is based on a presentation he gave at the 1984 OSA annual meeting.

average. Figure 1 shows the benefits of averaging pulses to bring "real" data out of the noise.

We have recorded more than 650 such vertical signal profiles throughout a three-year period beginning in May 1981, a period that fortuitously includes the El Chichón volcanic event. From these 600 profiles, nearly 260 were chosen for analysis on the basis of quality and temporal independence of the data.

After exhaustive system calibration, the backscatter signals were inverted by computer using the coherent lidar equation to produce vertical profiles of β, the volume backscatter coefficient. β has units of cross-sectional area per unit volume per steradian (isotropic scattering into a 4π steradian sphere is assumed), or m^{-1} sr^{-1} in MKS. A typical β value of 10^{-10} m^{-1} sr^{-1} is equivalent to one 40-μm diameter particle in 1 m^3. Scaled up, this corresponds to a single 1 mm diameter "particle" per house (500 m^3). Of course, atmospheric β values arise from particles of many different sizes and shapes, but contributions to our total signal are dominated by aerosols 1-2 μm in diameter.

Before averaging the β values observed during a 3-month period from a fixed altitude (to determine the seasonal average, for example), we must understand how the β values are distributed statistically. To do this we plot the ordered β values versus cumulative probability, with the probabilities (0-100%) on a Gaussian-spaced axis (dense near 50%, sparse near 0% and 100%).

A normally distributed variable would plot as a straight line on such a graph, but all of our plots were convex upward. However, by plotting the logarithm of β, we obtained straight lines for all but the lower altitudes, indicating that the logarithm of β is normally distributed. Averaging therefore should be done on $\log\beta$ (geometric averaging) and not on β itself (arithmetic averaging). Geometric averaging typically lowers mean values by a factor of 2.5 or so below mean values for arithmetic averaging for standard deviations typical of our data. The log-normal property of β points to multiplicative injection and mixing mechanisms[3], such as those associated with atmospheric convection[4] and cosmic mass distributions, and is not surprising.

A theoretical derivation, borrowed from economics (wealth is log-normally distributed in Western culture), sheds light on possible atmospheric processes at work. Let's begin with a source region for β of value β_1 and end with an observed β_n, having progressed through a series of n transformation in time and/or space. If the change in β from one step to the next is proportional to the previous value, then

$$\beta_{i+1} - \beta_i = \alpha_i\beta_i, \qquad i = 1,2,\ldots n.$$

The α_i are random, in general. Rewriting and summing gives

$$\sum_{i=1}^{n} \frac{\Delta\beta_i}{\beta_i} = \sum_{i=1}^{n} \alpha_i,$$

or for $\Delta\beta_i$ small and n large,

$$\int_{\beta_1}^{\beta_n} \frac{d\beta}{\beta} = \log\beta_n - \log\beta_1 = \alpha_1 + \alpha_2 \ldots + \alpha_n.$$

Then $\log\beta_n = \log\beta_1 + \alpha_1 + \alpha_2 \ldots + \alpha_n$ and $\log\beta_n$ is normally distributed by the Central Limit Theorem, being the sum of many random variables.

Figure 2 shows a cumulative probability plot typical of the mid-troposphere, together with the best straight-line fit. The mean β for this set can be found by transferring to the $\log\beta$ axis from the 50% probability point. Also, one can readily answer questions such as "What percent of the time is $\log\beta$ above (or below) a fixed value?" The standard deviation of the distribution is directly proportional to the slope of the straight line.

Averaging our data geometrically at each altitude for various seasons leads to profiles like those of Fig. 3, where the El Chichón stratospheric cloud is apparent. Notice how the cloud lowers and extends in height with time. Subsequent profiles show the cloud stabilizing at 17 km altitude and dissipating from the stratosphere while apparently increasing tropospheric β values. The mechanisms and rates for this stratosphere-troposphere exchange are currently being determined, but it is obvious that more than just gravitational settling is at work. Stratospheric/tropospheric folding[5] is a likely candidate to explain the observed vertical mixing.

Another method of displaying the data is to choose an altitude and plot the observed β values versus time, suitably

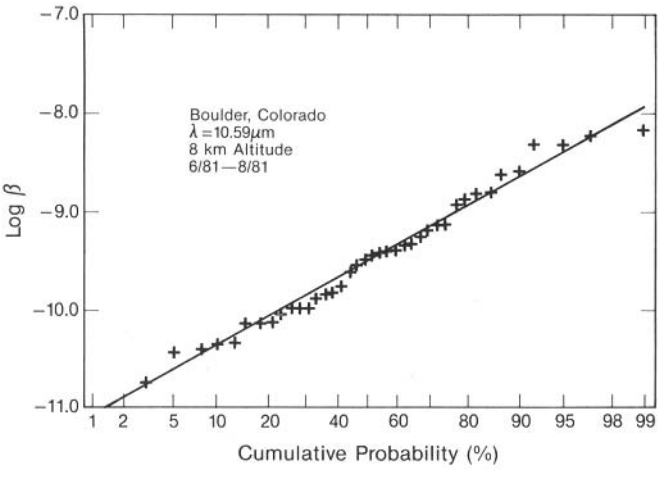

Fig. 2. Cumulative probability plot for $\log\beta$ at 8 km altitude for data observed in summer 1981 and the best straight-line fit. Median $\log\beta$ occurs at 50% probability, standard deviations at 16% and 84%. One may easily determine percentage of observations above or below a given level of $\log\beta$.

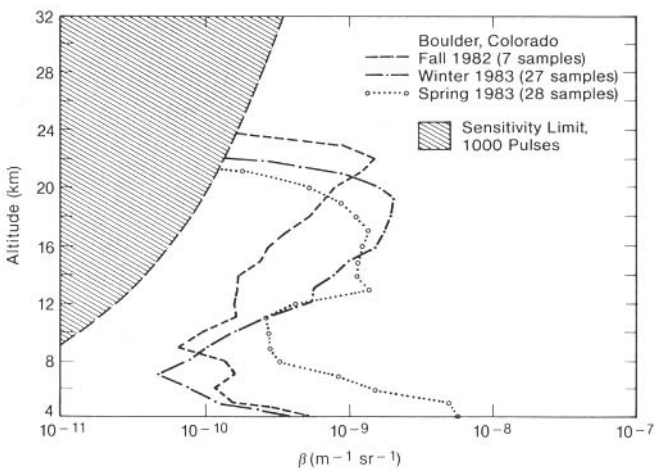

Fig. 3. Seasonally averaged profiles showing the appearance of the El Chichón cloud in the stratosphere in fall 1982 and its subsequent lowering and contamination of the troposphere.

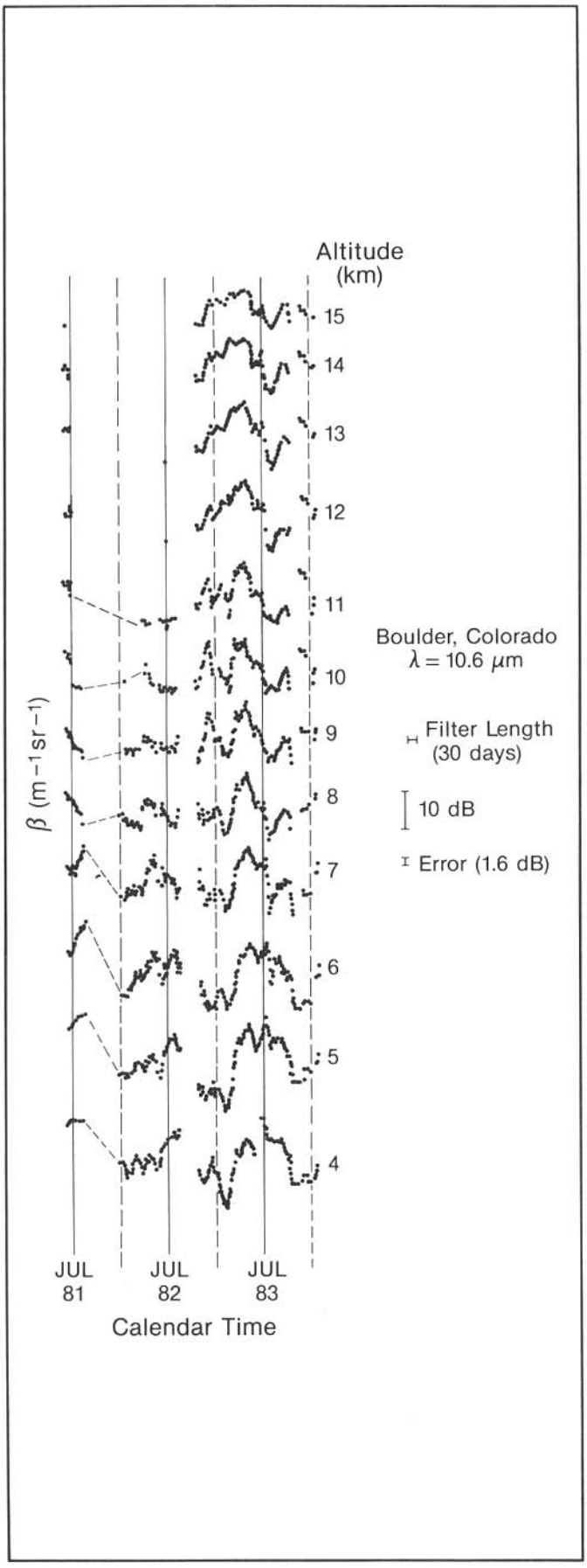

Fig. 4. Stacked time series showing both stratospheric and tropospheric backscatter and phasing relationships.

averaged with a running time filter. Such plots show marked cycles with both annual and semiannual periods. By stacking the time histories for a range of altitudes as in Fig. 4, we can note phase changes and other similarities and differences between altitude regimes. Quantifying these effects near the tropopause leads to better understanding of stratospheric purging.

Peaks in β that occur in the springtime lower troposphere hint to long-range Gobi dust transport (trajectory analyses are being performed) or to organic aerosol injection by plants. The organic injection hypothesis has been proposed[6] by the Smithsonian Astrophysical Observatory using its long-term solar aureole data, which display similar springtime maxima over many years.

We normally take data only when it appears visually that no clouds are overhead. However, even then we find that about 30% of the time one or more cirrus layers are present in the high troposphere. While the El Chichón stratospheric layer provided a background target that did not change over our 5-min observation period, we alternately took data with and without patchy cirrus in the beam. This technique enabled us to measure the attenuation coefficient α (m^{-1}) due to cirrus, while simultaneously sensing β (m^{-1} sr^{-1}). We found the ratio β/α lies between 10^{-4} and 10^{-3} (sr^{-1}), generally agreeing with our theoretical value[7] of $\alpha = 0.14L$ (km^{-1}) used in LOWTRAN 6, where L is the cirrus thickness (km). Backscatter coefficients are typically 10^{-8} to 10^{-7} (m^{-1} sr^{-1}) for thicknesses of 1-2 km, with depolarization strong in the lower portions of the layer, weak in the middle, and nearly gone at the top.[8]

(Continued on page 39)

Radiation Forces on Atoms

Nonlinear Optics

Integrated Optics

Fiber Gyroscopes

Journal of Lightwave Technology

Volume 3, No. 1 **February 1985**

(Continued from page 15)

Certainly NOAA is not the only group making atmospheric infrared β measurements, although our set is probably the most extensive to date. NASA's Marshall Space Flight Center has both cw and pulsed systems that operate either ground-based or airborne. The Jet Propulsion Laboratory has measured β profiles nearly simultaneously at both 9.3 μm and 10.6 μm wavelengths[9] and found a significant increase in β at all altitudes at 9.3 μm (this is predicted theoretically by refractive index resonance effects). The Royal Signal and Radar Establishment in England has been flying a cw airborne system[7] for several years, accumulating a large but unpublished data set on atmospheric β's.

For the future, more extensive measurement programs are planned to improve understanding of global variability so crucial to the WINDSAT concept. These efforts are being coordinated by NASA through a series of workshops. New systems that may become involved in these efforts include, among others, those being built by NASA Langley, the Air Force Geophysics Laboratory, CSIRO in Australia, and the University of Arizona. Although the NOAA set has provided some tasty morsels of knowledge that should help in designing the future experiments, the real feast will occur when the global data set is harvested and processed.

References

1. R.M. Huffaker, Ed., "Feasibility study of satellite-borne lidar global wind monitoring system," NOAA Tech. Memo. ERL WPL-37 (NOAA Environmental Research Laboratories, Boulder, Colo., 1978).
2. M.J. Post, R.A. Richter, R.M. Hardesty, T.R. Lawrence, and F.F. Hall Jr., Proc. Soc. Photo-Opt. Instrum. Eng. **300**, 60 (1982).
3. J. Aitchison, and J.A.C. Brown, *The Log-normal Distribution* (Cambridge U. Press, London, 1957).
4. R.E. Lopez, Mon. Weather Rev. **105**, 865 (1977).
5. M.A. Shapiro, "Turbulent mixing within tropopause folds as a mechanism for the exchange of chemical constituents between the stratosphere and troposphere," J. Atmos. Sci., **37**, 994-1004 (1980).
6. R.G. Roosen and R.J. Angione, "Atmospheric transmission and climate: results from Smithsonian measurements," Bull. Am. Meteorol. Soc., **65**, 950 (1984).
7. F.X Knelzys, E.P. Shettle, W.O. Gallery, J.H. Chetwynd Jr., L.W. Abreu, J.E.A. Selby, S.A. Clough, R.W. Fenn, "Atmospheric Transmittance/Radiance: Computer Code LOWTRAN 6," Chapter 7, AFGL-TR-83-0187, Air Force Geophysical Laboratory, Hanscom AFB, MA 01731 (1983).
8. A. Gross, M.J. Post, F.F. Hall Jr., "Depolarization, backscatter, and attenuation of CO_2 lidar by cirrus clouds," Appl. Opt. **23**, 2518-2522 (1984).
9. R.T. Menzies, M.J. Kavaya, P.H. Flamant, and D.A. Hamer, "Atmospheric aerosol backscatter measurements using a tunable coherent CO_2 lidar," Appl. Opt., **23**, 2511 (1984).